



Title	Theoretical solutions for strength-scaled unreinforced masonry for scaled soil-structure experimentation
Authors(s)	Laefer, Debra F., Erkal, Aykut, Cording, Edward J., Long, James H., Truong-Hong, Linh
Publication date	2010-07
Publication information	Laefer, Debra F., Aykut Erkal, Edward J. Cording, James H. Long, and Linh Truong-Hong. "Theoretical Solutions for Strength-Scaled Unreinforced Masonry for Scaled Soil-Structure." ASTM International, July 2010. https://doi.org/10.1520/JTE102420 .
Publisher	ASTM International
Item record/more information	http://hdl.handle.net/10197/3399
Publisher's statement	This is a preprint of an article published in Journal of Testing and Evaluation, 38 (4): 449-457, available at http://www.astm.org/DIGITAL_LIBRARY/JOURNALS/TESTEVAL/PAGES/JTE102420.htm
Publisher's version (DOI)	10.1520/JTE102420

Downloaded 2026-05-01 23:43:23

The UCD community has made this article openly available. Please share how this access benefits you. Your story matters! (@ucd_oa)



© Some rights reserved. For more information

Theoretical Solutions for Strength-scaled Unreinforced Masonry for Scaled Soil-structure Experimentation

Debra F. Laefer,¹ Aykut Erkal,² Edward J. Cording,³ James H. Long,⁴ and Linh Truong Hong⁵

¹Tenured Lecturer and Lead Principal Investigator, Urban Modelling Group (UMG), School of Architecture, Landscape, and Civil Engineering (SALCE), University College Dublin (UCD), Dublin 4, Ireland; Phone: 353-1-716-3226; Fax: 353-1-716-3297; e-mail: debra.laefer@ucd.ie

²Post-doctoral Researcher, UMG, SALCE, UCD, Dublin 4, Ireland; Phone: 353-1-716-3232; e-mail: aykut.erkal@ucd.ie

³Professor Emeritus, Department CEE, UIUC, Urbana, IL 61801, USA; Phone: 1-217-333-6938; e-mail: ecording@illinois.edu

⁴Associate Professor, Department of Civil and Environmental Engineering (CEE), University of Illinois at Urbana-Champaign (UIUC), Urbana, IL 61801, USA; Phone: 1-217-333-2543; Fax: 1-217-333-9464; e-mail: jhlong@illinois.edu

⁵Doctoral Student, UMG, SALCE, UCD, Dublin 4, Ireland; Phone: 353-1-716-3232; e-mail: linh.truong-hong@ucdconnect.ie

ABSTRACT: Reduced-scale masonry testing offers advantages of lower costs and shorter schedules compared to full-scale testing, but achieving results reflective of full-scale behavior requires development and fulfillment of appropriate scaling relationships. In many model-scale experiments, geometric scaling occurs but kinematic and/or dynamic similitude is not fully satisfied. This paper describes the theoretical basis and evolution of the equations necessary to achieve kinematic similitude for soil-structure testing at one-gravity for unreinforced masonry. Critical considerations relate to preventing the soil from being overloaded. By adopting a standard linear relationship of increased soil stiffness with depth, the controlling principle becomes the application of restricted, scaled loads throughout the entirety of the structure-soil system. As such, material strength and stiffness must be scaled accordingly to respond appropriately under the reduced stress. An example is provided for an adjacent excavation experiment with related empirical verification and computational quantification.

KEY WORDS: brick masonry, mortar, laboratory testing, soil-structure, scaling, sand, adjacent excavation, cracks, historic preservation, non-cohesive soil

Introduction

Testing scaled-masonry systems is advantageous when a problem is too complex for an analytical solution or too unwieldy for full-scale testing [1,2]. Scaled models allow cost-effective, multi-parameter exploration, but soil-structure experiments must address reduced soil strength and stiffness due to shallow soil depths. Therefore, at one-gravity (1g), engineering properties of scaled-building components must be modified to compensate for the lower allowable soil stresses to generate realistic building responses to soil displacements. Reactions at scaled-loads must be akin to reactions of the prototype behaving under full loading. This paper presents the fundamentals of soil-structure scaling for 1g models, along with an example for an adjacent excavation experiment conducted at a 1/10th scale.

Backgrounds

Scaling

Experiments at less than full-size may generate incorrect responses. Langhaar [3] named these negative repercussions “scale-effects”. Scale-effects may emerge in terms of geometric, kinematic, and/or dynamic factors. To minimize (and eliminate, where possible) scale-effects when conducting model-scale work, the concept of dimensional homogeneity or similitude was pioneered by Buckingham [4] and Rayleigh [5] and furthered by Langhaar [3]. Specifically, prototype behavior must be understood so that variables exhibiting a significant influence on system performance can be identified as the input components of dimensionless products to describe the behavior of both the model and prototype [6]. Significant variables are then considered in relation to components of mass, time, and length. A series of linear equations (one each for mass, time, and length) are established using a series of unknown constants for each

performance variable of significance (e.g. density, velocity). Various arrangements are tried in order to establish a determinant for a 3x3 group. The determinant is considered the rank. The difference between the rank and number of performance variables establishes the required number of independent, dimensionless products. According to Langhaar [3], dimensionless products are independent, “If every other dimensionless product of the variables is a product of powers of dimensionless products in the set.” These are achieved through solving the resulting linear equations by setting all excess variables equal to zero, except the variable of interest; usually the one over which there is greatest control [7]. For the research described herein, these experimental variables related to geometry, applied loading, and masonry strength and stiffnesses.

Prior Solutions

Meeting kinematic and dynamic, as well as geometric similitude can be achieved variously depending upon the physical constraints of the experiments. For shake-table testing, one solution is to increase applied loads [8]. With centrifuge testing, accelerations are increased with appropriate material property modifications. In 1g testing, many researchers have ignored scaling requirements because of the difficulty in manufacturing small-scale units and constructing assemblages of reduced-strength material, thus potentially introducing unintended scale-effects.

As an example of the state of practice, shear testing of 1/3rd scale wall assemblages by Neto et al. [9] used full-strength materials. Cracking processes and patterns matched full-scale testing, but scaled-samples over-predicted shear capacity by 94%. Similarly, 1/10th scale shake table work by

Turer et al. [10] on masonry seismic strengthening employed cut, light-weight marble because 1/10th scale, hollow-clay brick units could not be traditionally manufactured. Additionally, a clayey soil representative of local practices served as the mortar. The observed crack patterns from this testing were similar to field cases, but performance enhancement could only be qualitatively extrapolated to full-scale.

To date only limited studies have been conducted to investigate the behavior of masonry structures incorporating small-scale masonry models. Harris and Sabnis's nearly exhaustive treatment of the topic for concrete and block masonry structures, does not address brick masonry [7]. Additionally, although similitude-based strength modeling of concrete block masonry is relatively well-established (compared to brick masonry) and relatively capable of predicting prototype behavior [11,12], the techniques and methods are not fully transferable to brick masonry because of the complicated relationship in brick/mortar bonding [13]. Furthermore, specific studies conducted on brick masonry modeling remain limited [14,15,16]. Specifically, geometrically scaled models have lacked strength scaling, and even when low strength bricks were created [17], no procedural basis was presented to establish a consistent and robust methodology from which to do further modeling or to verify the results short of full-scale prototype testing. As early as 1982, Mark [18] writes about the importance of similitude and strength-scaling in modeling of masonry, but chooses to avoid the laboratory challenges by adopting photo-elastic analysis in plastics.

To facilitate strength-scaling options for soil-structure experiments, results of a new study using modified materials are presented herein. The theoretical relationships developed are included below, along with the affiliated experimental results.

Soil-structure Scaling

Soil strength and stiffness pose challenges to scaled geotechnical research, especially when the testing includes actual structures or structural components, because model-scale dimensions result in decreased soil depth (i.e. testing chambers are not as deep as actual prototypes). Thus, the resulting soil strength and stiffness are less than those of the prototype soil. Therefore, applied loads must be reduced to prevent soil overloading. Equations describing stress, strain, and strength are satisfied by either modifying the geometry or altering performance characteristics of the experimental materials. Since strains result from changes in stress and stiffness, strain parity is often recommended [19,20] for representing equivalency between the model and prototype (Eq. 1)

$$\varepsilon_p = N \varepsilon_m \quad (1)$$

where ε_p = prototype strain, ε_m = model strain, and N = scale factor.

In non-cohesive soils, bearing capacity and deformability are assumed to be linear with depth (Eq. 2 and 3), as proposed by Terzaghi [21], where q_a is net allowable load, q_d design load, SF safety factor, γ soil unit weight, D_f foundation depth factor, B foundation width factor, and N_c and N_q dimensionless bearing-capacity factors depending primarily on the soil's friction angle.

Stress, σ_s , at a point is proportional to the soil's elastic modulus E_s , unit weight γ , and depth H .

$$q_a = \frac{q_d}{SF} = \left[\frac{\gamma N_\gamma}{2} + \gamma (N_q - 1) \frac{D_f}{B} \right] \frac{B}{SF} \quad (2)$$

$$\sigma_s \propto E_s \propto \gamma H \quad (3)$$

Based on Eq. 2 and Eq. 3, the soil characteristics are considered linear. Thus, because the experimental set up used in this laboratory study was only 1/10th the size of the prototype, the soil was considered to be only 1/10th as strong and 1/10th as stiff at a model depth as that of the prototype (assuming all loading remains within the material's elastic range, an appropriate assumption for achieving the study's aims [9]). Changing soil characteristics by soil modification (e.g. heavy-particles or synthetic soils) is possible but rarely adopted [22] because of the required volume of material and the desire to model other soil-related parameters. Consequently, the soil could only be loaded to 1/10th of that of the prototype (Eq. 4),

$$\left(\frac{q_a}{q_d} \right)_p = \left(\frac{q_a}{q_d} \right)_m \quad (4)$$

For building foundations with elastic stiffness, Eq. 5 is applicable to model displacement (δ) and allows geometric or mechanical property modification to achieve similitude,

$$\left(\frac{\delta}{B}\right)_m \propto \left(\frac{q_f}{E_s}\right)_m \quad (5)$$

where q_f is the foundation load and B the foundation width. To achieve strain equivalency (Eq. 6), model building stiffness should be reduced (Eq. 7), because applied stresses in the model buildings are only $1/10^{\text{th}}$ of the prototype because of the soil loading limit.

$$\left(\frac{\sigma}{E}\right)_p = \left(\frac{\sigma}{E}\right)_m \quad (6)$$

$$(E_s)_p = 10 \times (E_s)_m \quad (7)$$

Since loads on the model are transferred to the soil, stresses applied to the soil are the same as those on the model building's foundations (Eq. 8),

$$\sigma_{ss} = \sigma_b \quad (8)$$

where σ_{ss} is the applied stress on the soil surface, and σ_b is the stress applied through the building components at the soil-structure interface. Consequently, strain equivalence at the soil-structure interface can be written by Eq. 9, with the help of Eq. 8,

$$\left(\frac{1/10 \sigma_{ss}}{1/10 E_s}\right)_p = \left(\frac{\sigma_{ss}}{E_s}\right)_m = \left(\frac{P/A_b}{E_b}\right)_m \quad (9)$$

where E_b is the building's Young's Modulus and A_b its loaded area (assumed to be uniformly loaded). From Eqs. 6-8, to meet the challenges of matching soil characteristics, model building materials must be manufactured with ultimate load capacities and stiffnesses of only $1/10^{\text{th}}$ of those of the full-scale prototype, if the model-scale system is to respond under $1/10^{\text{th}}$ prototype loads as the prototype would under full loading (Eq.10).

$$\frac{1}{10}(E_b)_p = (E_b)_m \quad (10)$$

An experimental example of these principles is provided below.

EXAMPLE

The testing program reported herein investigated the impact of adjacent excavation related soil movement on existing structures (Fig. 1). Major variables included excavation-wall stiffness, applied-load level, and building structural systems. This work is a subset of a larger testing program [23,24]. Experiments were conducted in a purpose-built, reconfigurable testing chamber (4.90m x 4.30m—in plan, 3.00m—in depth, containing 1400kN of pluviated, poorly-graded sand). The testing chamber was formed by concrete blocks post-tensioned vertically and laterally to provide a high level of rigidity and safety (Fig. 1). Six tests were conducted, each with a continuous sheet-piling wall (set 0.76m from the chamber's front), with 3 levels of tied-back anchors, a pair of model buildings walls, and a free field area (Fig. 1). Because $1/10^{\text{th}}$ scale was the largest possible scale that could be incorporated without incurring boundary condition

influence problems, significant consideration to achieving similitude was critical to avoid scale-effects at this relatively small size.

There were two physical tests (Test 4 and Test 5) conducted to investigate the response of unreinforced masonry (URM) subjected to excavation-induced ground movements. In each physical test, a pair of URM walls [East and West (Table 1)] were embedded in the sand. These walls were designed to be representative of a class of structures namely low-rise, unreinforced masonry as typical of American vernacular and small commercial construction in late 19th and early 20th century architecture, as opposed to modeling a specific building. The URM walls in Test 4 and Test 5 were supported by shallow and deep footings, respectively. Various load levels and distributions were applied to the four model walls as shown in Fig. 2 and summarized in Table 2. For collecting precise results, special attention was paid to installation and instrumentation details. Mounting details showing Plexiglas sleeves to assist in the seating of the applied loads were used both at the windows and along the tops of the wall seen in Fig.s 2 and 3. Over each brick, along the wall's top, a 50.8mm Plexiglas sleeve (Fig.s 2 and 3) was set with a slight space between it and the next sleeve, to avoid unintentional stiffening of the wall. Atop each Plexiglas sleeve, the load was applied. The sleeve was designed to prevent the out-of-plane support system from getting caught in the wall's mortar joints as the wall displaced against the support (Fig 2). Lead or steel blocks (depending upon desired loading levels) were mounted with construction adhesive atop each sleeve as dead load (Fig. 3). Footing-level loads were affixed with construction adhesive so that they were adhered to the brick through a chair assembly and not directly on the footings (Fig. 2). Along the masonry wall's front, lead pieces (51mm x 76mm

x 8mm) were attached to individual bricks to preserve system stiffness by epoxying velcro to the bricks and lead. This permitted the epoxy to obtain full strength prior to loading (Fig. 4).

The dead load ranged from 90.72kg (double the model's weight) to 181.44kg resulting in 24.82kPa – 49.64kPa in applied pressure. These load levels were determined from Kidder [25] and similar early codes. Data was collected on the masonry walls at levels 1, 2, and 3 along points a, b, c and d for a total of 12 measurements points.

The soil was a locally obtained sand from Pekin, Illinois and categorized as a clean, medium grained, uniform sand with mostly rounded to sub-rounded particles (qualifying as SP under the Unified Classification System with a coefficient of uniformity of 2.64 and coefficient of curvature of 1.12). The sand was washed and kiln dried prior to usage.

The excavation wall consisted of a 2.5mm thick, steel sheet plate, with three levels of tieback anchors (6.5 mm diameter, stainless steel rods with their unbonded zone covered with a plastic sleeve). The excavations were done progressively in 15 stages. In each stage, either the system was post-tensioned or a depth of approximately 10.16 cm of soil was removed from in front of the “wished in place” tieback excavation wall; meaning that during the experimental set up the wall was embedded and the sand back filled around it, instead of being installed simultaneously with the excavation, which was necessary because of the extensive instrumentation on the wall. The post-tensioning occurred at pre-designated depths in the excavation wall. Prior to those points in the testing cycle, the tieback anchors were in the testing chamber but not loaded. Test readings of all elements in the experiments were taken before and after loading, as well as during

delays of 2 hours or more in the testing cycle. A total of 15 excavation and anchor stressing stages were conducted to reach the final design grade, H_{dg} . During full-scale excavations, two stages are often considered critical. One is immediately prior to the installation of the first lateral support (referred to as stage 3 heretofore). The other is the performance stage, when the excavation has reached its design depth, often called “design grade” (referred to as stage 15 heretofore). Thus, these will be the focus of the data reporting. After verification (see below) the results of these tests were compared to subsequent numerical modeling to demonstrate the potential development of scale effects for non-strength scaled materials.

Verification of Experimental Model

To show the validity of the results, the following sections compare the experimental results to expected empirical outcomes with respect to vertical soil settlement, building displacement, and building damage. Figure 5 depicts soil settlement profiles from the free field side scaled by a factor of 10, where S_v is the vertical settlement, d is the lateral wall displacement at the top, and H_{dg} is the height at design grade, representing the deepest point of excavation. As shown in fig. 5, the resulting vertical soil settlement profiles are in agreement with the extent and shape of those proposed by Peck [26] for installations of average workmanship in sand.

In the geotechnical community, it is regularly assumed that free field soil settlement is approximately equal to the building response during adjacent excavations [e.g. 27]. Such a response is shown in Fig. 6 where foundation level vertical displacement is plotted in comparison to surface soil settlement for both model walls at both stages of reported testing; these results are representative of the overall testing program. In Stage 3, the walls had yet to be

mobilized as soil movement was small. In Stage 15, the wall with the deep foundations (T5W) moved less with the soil than the more easily transported wall with shallow foundations (T4E). In all cases, the wall displacements with respect to the soil movements were reasonable and within the expected range of responses.

Having now established that the vertical soil profiles were of the expected shape and magnitude and that these soil displacement profiles generated expected building displacements, the third and final validation step was in assessing how the expected building damage levels compares to that recorded from the URM model walls. This was done through the application of angular strain limits.

Angular strain was defined by Burland and Wroth [28] as a summation of the tangents with respect to both deflected sides of a point in Eq. 11 (Fig. 7).

$$\alpha = \frac{\delta_{BA}}{l_{AB}} + \frac{\delta_{BC}}{l_{BC}} \quad (11)$$

According to Rankin's damage criteria [29] using angular strain α , damage is negligible for values $\alpha < 0.002$, slight for $0.002 < \alpha < 0.005$, moderate for $0.005 < \alpha < 0.020$, and severe for $\alpha > 0.020$. In the above described study, angular strains α were measured at two points at the base of the model walls. Cracking began prior to loading the first tie-back (Stage 3) and tended to worsen as the excavation proceeded. Angular strains and maximum crack sizes are presented with corresponding damage levels in Table 3. Based on the calculated angular strains and Rankin's damage prediction scale, no damage was predicted for either building for Stage 3 and

moderate damage was predicted for both buildings at Stage 15 (Table 3). Actual damage levels were determined by measuring crack width, a common method to evaluate building response [30]. The damage level was assigned based on width limits proposed by Burland et al. [30]. At Stage 15, strong agreement between the expected and actual damage was achieved. Earlier in the testing cycle recorded damage was slightly more than the predicted damage. This exercise demonstrates that the vertical soil displacements, subsequent building displacements, and affiliated building damage were all in good agreement with empirical expectations.

To better illustrate the resulting divergence of when scaling relationships are not honored, numerical modeling was conducted. A comparison of strength-scaled and non-strength-scaled materials applied to the 1/10th scale experimental work is presented below.

Numerical Modeling

Non-linear analysis was performed using ANSYS® V11.0. Throughout the model, the 3D element Solid65 was employed. The element was defined by 8 nodes, each having 3 degrees of freedom. Every isotropic element had 2 x 2 x 2 integration points and was capable of cracking in tension and crushing in compression. A micro-modeling strategy was embraced, in which brick and mortar were modeled separately, with the assumption of perfect bonding between bricks and mortar as is commonly considered [e.g. 31]. The micro-model consisted of 18,248 nodes and 9,373 elements (Fig. 8). A smeared crack model was used to predict the cracking across the masonry.

Additionally, in studying the contact between two bodies, the surface of one body is conventionally taken as a contact surface and the surface of the other body as a target surface. In order to replicate the contact behavior of the lintels over the windows and the footings under the walls, Target170 (used to represent 3-Dimensional target surfaces for associated contact elements) and Contact173 (used to represent contact and sliding between 3-D target surfaces and a deformable surface defined by this element) were employed. The lintel was allowed to slide freely, but a Coulomb friction model was applied to represent the interaction between the wall and footing. Furthermore, as failure through other elements was not expected, element Solid45 (a 3D solid element with 8 nodes each with 3 translational degrees of freedom) was used to model the lintels and footings. Mechanical material properties, as established through small sample testing, were used as the input values for tensile and compressive strength and strain characteristics for the strength-scaled model (Table 4). Non-strength-scaled (i.e. prototype) kinematic values were used for the non-strength-scaled material inputs, thus only scaling the geometry.

In both the strength-scaled and non-strength-scaled cases, the numerical model was subjected to the same gravity loads [self-weight and applied, static, vertical loads (Table 2)], along with the same excavation-induced displacements obtained from the experimental program. In the first loading phase, gravity loads were applied to the model and the bottom of the footings were fixed. This allowed stress to develop in the model but without displacement. The loaded, non-displaced condition was considered akin to the in-situ situation of existing structures, when displacement measurements are taken just prior to construction activities. Subsequently, excavation-induced building displacements of each construction stage in the physical test were numerically imposed

at the bottom of each wall [24]. Physical testing constraints limited the number of data collection points. The numerical results were reported in a corresponding manner. In general, masonry buildings are thought to behave as rigid bodies (see Fig. 10) Thus, more continuous documentation is rarely justified.

Numerical modeling of the strength-scaled and non-strength-scaled materials (Table 5) were compared to the experimental results for Tests 4E and 5W. The horizontal and vertical displacements on the top of the building walls are shown (with horizontal depicted as positive and vertical as negative), in Figures 9 and 10 respectively, with the numerical displacement outputs tabulated in Tables 6 and 7. Interestingly, scale effects only emerged significantly in the vertical displacement of the corner furthest from the excavation. In Test 4E, the discrepancy using the non-strength-scaled (or prototype) mechanical properties was 448% at that point. In contrast, the difference for the strength-scaled FEM results was only 17%. For the heavier URM wall used in Test 5W, the general performance of the non-strength-scaled model was similarly poor in predicting the vertical response. In that test, wall displacement for the non-strength-scaled material exhibited displacements at the front corner (arguably the most critical point in the modeling as this is where field monitoring is concentrated) differed by more than 16%. Two of the other three points were well in excess of this, with the back corner differing by 209%. In contrast, the numerical modeling of the strength-scaled materials had displacements that were nearly all within 10% of the physical model, and the back corner only differed by 24%. This achieved accuracy with the strength-scaled material is within the expected coefficient of variation of $\pm 20\%$ for unreinforced masonry [32].

Conclusions

To achieve scalable responses when testing less than full-scale masonry, kinematic, as well as geometric, similitude relationships must be upheld. This paper provides essential theoretical principles for soil-structure scaling in 1g geotechnical experimentation, including a representative set of sample masonry wall buildings subjected to adjacent excavation. In this study, strain parities were selected as the basic dimensionless grouping for the experimentation. This dictated that material properties had to be modified to accommodate the lower applied loads required by the reduced soil depth. In the example provided, the geometric scaling factor of $1/10^{\text{th}}$ was related directly to the stress and subsequently applied to the components of the model buildings' strength and stiffness to properly accommodate the reduced applied stress. Numerical analysis further emphasized the necessity to adhere to the often over-looked requirement of kinematic scaling during 1g testing to ensure appropriate response, which was shown to differ by more than two orders of magnitude when compared to the physical tests when strength scaling was ignored.

Acknowledgments

The experimental work was made possible through generous funding by the Schnabel Foundation Company, the National Science Foundation CMMI9713854, and UIUC's Department of Civil and Environmental Engineering and realized through the tireless dedication of several dozen undergraduates. The computational portion of this work was made possible through the funding of Science Foundation Ireland (SFI/PICA/I850).

References

[1] Schuring, J. S., *Scale Models in Engineering, Fundamentals and Applications*, Pergamon Press, Oxford, England, 1977.

[2] Wood, D. M., *Geotechnical Modelling*, Spon Press, Oxfordshire, 2004.

[3] Langhaar, H., *Dimensional Analysis and Theory of Models*, John Wiley & Sons, Inc., New York, NY, 1951.

[4] Buckingham, E., "On Physically Systems: Illustrations of the Use of Dimensional Equations," *Physics Reviews* 4, 1914, pp. 345-376.

[5] Rayleigh Lord, (J. W. Strutt), "The Principle of Similitude," *Nature* 95, 1915, pp.66-68.

[6] Shaughnessy, E. J., Katz, I. M. and Schaffer, J. P., *Introduction to Fluid Mechanics*, Oxford University Press, Oxford, England, 2005.

[7] Harris, H. G. and Sabnis, G. M., *Structural Modeling and Experimental Techniques*, CRC Press, Florida, USA, 1999.

[8] Lu, X., Zou, Y., Lu, W. and Zhao, B., “Shaking Table Model Test on Shanghai World Financial Center Tower,” *Earthquake Engineering and Structural Dynamics*, Vol. 36, No. 4, 2007, pp. 439-457.

[9] Neto, C., Correa, M. and Ramalho, M., “Proposal of a Test Specimen to Evaluate the Shear Strength of Vertical Interfaces of Running Bond Masonry Walls,” *Canadian Journal Civil Engineering*, Vol. 35, No. 6, 2008, pp. 567-573.

[10] Turer, A., Korkmaz, S. and Korkmaz, H., “Performance Improvement Studies of Masonry Houses Using Elastic Post-tensioning Straps,” *Earthquake Engineering and Structural Dynamics*, Vol. 36, No. 5, 2007, pp. 683-705.

[11] Hamid, A. A., Abboud, B.E. and Harris, H.G., “Direct Modelling of Concrete Block Masonry under Axial Compression,” *Masonry: Research, Application, and Problems, ASTM STP 871*, J.C. Grogan and J.T. Conway, Eds., American Society for Testing and Materials, Philadelphia, 1985, pp. 151-166.

[12] Abboud, B. E., Hamid, A. A. and Harris, H. G., “Small-Scale Modeling of Concrete Block Masonry Structures,” *ACI Structural Journal*, Vol. 87, No. 2, 1990, pp.145-155.

[13] Ribar, J. W. and Dubovoy, V. S., “Investigation of Masonry Bond and Surface Profile of Brick,” *Masonry Materials: Design, Construction and Maintenance, ASTM Special*

Technical Publication 992, Ed. H. A. Harris, American Society for Testing and Materials, Philadelphia, PA, 1988, pp. 33-37.

[14] Angelillo, M. and Olivito, R. S., “Experimental Analysis of Masonry Walls Loaded Horizontally in Plane,” *Masonry International*, Vol. 8, No. 3, 1995, pp. 91-100.

[15] Cavicchi, A. and Gambarotta L., “Collapse Analysis of Masonry Bridges Taking into Account Arch-fill Interaction,” *Engineering Structures*, Vol. 27, No. 4, 2005, pp. 605-615.

[16] Royles, R. and Hendry, A. W., “Model Tests on Masonry Arches,” *Institution of Civil Engineers Proceedings*, Part 2, 1991, pp. 299-321.

[17] Egermann, R., Cook, D. A. and Anzani, A., “An Investigation into the Behaviour of Scale Model Brick Walls” *Brick and Block Masonry*, Vol. 1, 1991, pp. 628-635.

[18] Mark, R., *Experiments in Gothic Structure*, MIT Press, Cambridge, London, 1982.

[19] Zarnic, R., Gostic, S., Crewe, A. and Taylor, C., “Shaking Table Tests of 1:4 Reduced-scale Models of Masonry Infilled Reinforced Concrete Frame Buildings,” *Earthquake Engineering and Structural Dynamics*, Vol. 30, No. 6, 2001, pp. 819-834.

[20] Tomazevic, M. and Klemenc, I., “Verification of Seismic Resistance of Confined Masonry Buildings,” *Earthquake Engineering and Structural Dynamics*, Vol. 26, No. 10, 1997, pp. 1073-1088.

[21] Peck, R. B., Hanson W. E. and Thornburn, T. H., *Foundation Engineering*, 2nd Edition, 1974.

[22] Stanier, S. A., “Geotechnical Modeling Using a Transparent Synthetic Soil,” *CIV300 Final Report, Department of Civil and Structural Engineering*, University of Sheffield, UK, 2006.

[23] Laefer, D. F., “Prediction and Assessment of Ground Movement and Building Damage Induced by Adjacent Excavation,” *Ph.D. Thesis*, University of Illinois at Urbana-Champaign, Urbana, IL , 2001.

[24] Hong, T. H. and Laefer D. F., “Micro vs. Macro Models for Predicting Building Damage Underground Movements,” *The International Conference on Computational Solid Mechanics*, Hochiminh City, Vietnam, November 27-30, 2008, pp. 259-268.

[25] Kidder, F. E., *The Architects' and Builders' Pocket Book*, John Wiley and Sons, Inc., New York, 1916.

[26] Peck, R. B., “Deep Excavation and Tunneling in Soft Ground,” Proceedings 7th International Conference Soil Mechanics and Foundation Engineering, State-of-the-Art-Volume, Mexico City, 1969, pp. 225-290.

[27] Laefer, D. F., Ceribasi, S., Long, J. H. and Cording, E. J., “Predicting Reinforced Concrete Frame Response to Excavation Induced Settlement,” Journal Geotechnical and Geoenvironmental Engineering, ASCE, 2009, Doi: [http://dx.doi.org/10.1061/\(ASCE\)GT.1943-5606.0000128](http://dx.doi.org/10.1061/(ASCE)GT.1943-5606.0000128)

[28] Burland, J. B. and Wroth, C. P., “Settlement of Buildings and Associated Damage.” Proceedings Conference Settlement of Structures, Pentech, London, 1974, Cambridge, England, 1975, pp. 611-654.

[29] Rankin, W. J., “Ground Movements Resulting from Urban Tunnelling: Predictions and Effects,” Engineering Geology of Underground Movements. Edited by Bell, F.G., Colshaw, M.G., Cripps, J.C., and Lovell, M.A. Geological Society, London, 1988, pp. 79-92.

[30] Burland, J. B., Broms, B. B. and de Mello, V. F. B., “Behavior of Foundations and Structures,” Proceedings, 9th International Conference Soil Mechanics and Foundation Engineering, II, State-of-the-Art Report, Tokyo, 1977, pp. 495-546.

[31] Anthoine, A., “Homogenization of Periodic Masonry: Plane Stress, Generalized Plane Strain or 3D Modelling?,” *Communications in Numerical Methods in Engineering* Vol. 13, No. 5, 1997, pp. 319-326.

[32] Brencich, A. and Felice, G.de, “Brickwork under Eccentric Compression: Experimental Results and Macroscopic Models,” *Construction and Building Materials*, 2008, doi:10.1016/j.conbuildmat.2008.09.004.

Tables

Table 1. Summary of dimensional characteristics of the prototype and the scaled model

Aspects	Prototype	Scale model
Excavation depth (m)	12.192	1.219
Lot width (m)	7.620	0.762
Lot depth (m)	24.384	2.438
Building width (m)	6.096	0.610
Building depth (m)	18.300	1.830

Table 2. Summarized vertical loads on the scale model test

Aspects	Test 4E	Test 4W	Test 5E	Test 5W
Self-weight building (N)	444.98	444.98	444.98	444.98
Top building (N)	889.64	1779.29	889.64	1779.29
Top windows (N)	222.41	222.41	0.00	222.41
Bottom window (N)	222.41	222.41	222.41	222.41
Footings (N)	222.41	222.41	222.41	222.41
Extra load on the front chair (N)	22.24	22.24	44.48	44.48
Façade load (N)	88.96	88.96	88.96	88.96
Total external loads (N)	1668.07	2557.72	1467.9	2579.96

Table 3. Results of deformation analysis; values at the base of the wall, where H_{dgi} is the design grade height for the specific test

Test	Test step	Calculated Angular Strain		Expected Damage		Actual Damage (According to Max Crack Width)		
		α_b	α_c	α_b	α_c	Bay ab	Bay bc	Bay cd
Test 4E	0.25 H_{dg4} (Stage 3)	-0.00059	-0.00028	No damage	No damage	Moderate (1.0 mm)	Slight (0.5 mm)	Moderate (1.0 mm)
	1.00 H_{dg4} (Stage 15)	-0.00770	-0.00568	Moderate	Moderate	Moderate (1.0 mm)	Slight (0.5 mm)	Moderate (1.0 mm)
Test 5W	0.16 H_{dg5} (Stage 3)	-0.00021	-0.00008	No damage	No damage	Slight (0.5 mm)	Slight (0.3 mm)	Slight (0.3 mm)
	1.00 H_{dg5} (Stage 15)	-0.00758	-0.00340	Moderate	Slight	Slight (0.5 mm)	Slight (0.3 mm)	Slight (0.5 mm)

Table 4. Mechanical properties of the masonry components

Aspects	Brick	Mortar	Lintels
Dimensions (mm)	57.86x 15.24x 29.75	3.21 ^(a) , 2.25 ^(b)	1.58
Mass density (kg/m ³)	1,783.9	1,557.9	674
Compressive strength (MPa)	8.446	1.310	N/A
Tensile strength (MPa)	1.262	0.152	N/A
Elastic modulus (MPa)	88.8	27.58	11,700
Poisson's ratio	0.25	0.30	0.25

* Note: (a) Head joint thickness; (b) Bed joint thickness

Table 5. Mechanical properties of prototype materials

Property	Prototype	Target	Actual (average)
Brick compressive strength (tested longwise, no end preparation)	41.37-55.16 MPa	4.14-5.52 MPa	4.43 MPa
Brick compressive strength (tested flatwise, no end preparation)	Not modeled due to lack of correlation between testing orientations	Not modeled	8.4 MPa
Brick modulus of rupture	8.62 MPa	0.86 MPa	0.39 MPa
Brick Poisson's ratio	0.30	0.30	0.25
Brick absorption	No modeling needed	Not modeled	16.3%
Brick mass density	No modeling needed	Not modeled	1783.9 (Kg/m ³)
Brick Young's modulus	No prototype data available	Not modeled	88.88 MPa
Brick tensile strength	No prototype data available	Not modeled	5.00 MPa
Mortar compressive strength	6.89 MPa	0.69 MPa	1.31 MPa
Mortar tensile strength	1.37 MPa	0.13 MPa	0.15 MPa
Mortar Young's modulus	6894.76 MPa	689.48 MPa	27.58
Mortar Poisson's ratio	No prototype data available	Not modeled	0.30
Mortar mass density	Not modeled	Not modeled	1,557.9 Kg/m ³
Masonry compressive strength for 5 brick high prisms	22.34-23.99 MPa	2.23-1.71 MPa	4.14 MPa
Masonry Young's modulus	7763.50-10342.14 MPa	772.21-1034.21MPa	1482.37MPa
Masonry shear strength	0.38-0.53 MPa	0.04-0.05 MPa	0.05 MPa
Masonry flexural bond	0.59-0.82 MPa	0.06-0.08 MPa	Untestable

Table 6. FEM results from scaled and unscaled materials compared to experimental response for Test 4E

Test 4E	Location on building (mm)			
	0	610	1220	1830
Arrangement				
Physical model horizontal disp. (mm)	4.953	4.839	5.037	4.521
Physical model vertical disp. (mm)	5.969	3.940	1.321	-0.127
FEM scaled material horizontal disp. (mm)	4.368	4.353	4.196	4.147
FEM scaled material vertical disp. (mm)	5.348	3.480	1.447	-0.149
<i>Absolute error horizontal disp. (%)</i>	<i>11.81</i>	<i>10.04</i>	<i>16.70</i>	<i>8.28</i>
<i>Absolute error vertical disp. (%)</i>	<i>10.40</i>	<i>11.66</i>	<i>-9.56</i>	<i>-17.32</i>
FEM Prototype (unscaled) material horizontal disp. (mm)	4.603	4.598	4.489	4.417
FEM Prototype (unscaled) material vertical disp. (mm)	5.598	3.565	1.269	-0.696
<i>Absolute error horizontal disp. (%)</i>	<i>7.07</i>	<i>4.97</i>	<i>10.87</i>	<i>2.30</i>
<i>Absolute error vertical disp. (%)</i>	<i>6.22</i>	<i>9.50</i>	<i>3.90</i>	<i>-448.03</i>

Table 7. FEM results from scaled and unscaled materials compared to experimental response for Test 5W

Test 5W	Location on building (mm)			
	0	610	1220	1830
Arrangement				
Physical model horizontal disp. (mm)	3.505	3.479	3.429	2.951
Physical model vertical disp. (mm)	5.012	2.142	0.631	-0.281
FEM scaled material horizontal disp. (mm)	3.814	3.730	3.356	3.271
FEM scaled material vertical disp. (mm)	4.556	2.357	0.650	-0.349
<i>Absolute error horizontal disp. (%)</i>	<i>-8.82</i>	<i>-7.23</i>	<i>2.12</i>	<i>-10.84</i>
<i>Absolute error vertical disp. (%)</i>	<i>9.10</i>	<i>-10.03</i>	<i>-2.99</i>	<i>-24.20</i>
FEM Prototype (unscaled) material horizontal disp. (mm)	3.860	3.790	3.720	3.308
FEM Prototype (unscaled) material vertical disp. (mm)	4.190	2.191	0.379	-0.869
<i>Absolute error horizontal disp. (%)</i>	<i>-10.13</i>	<i>-8.95</i>	<i>-8.48</i>	<i>-12.10</i>
<i>Absolute error vertical disp. (%)</i>	<i>16.40</i>	<i>-2.28</i>	<i>39.92</i>	<i>-209.25</i>

Figure Captions

Fig. 1. Testing chamber (adapted from [15])

Fig. 2. Model wall fully load, instrumented, and awaiting testing

Fig. 3. Dead load applied along the top of the model wall shown in Fig. 2

Fig. 4. Velcro pads shown epoxied to individual bricks as receptacles for dead load applied at the wall's façade location

Fig. 5. Soil surface settlement (after [18])

Fig. 6 Vertical (y) displacement variation across T5W and T4E at Stages 3 and 15

Fig. 7. Definition of angular strain

Fig. 8. Finite element model in ANSYS® simulated the reduced-scale model test

Fig. 9. Displacements along top of building during Test 5W

Fig. 10. Displacements along top of building during Test 4E

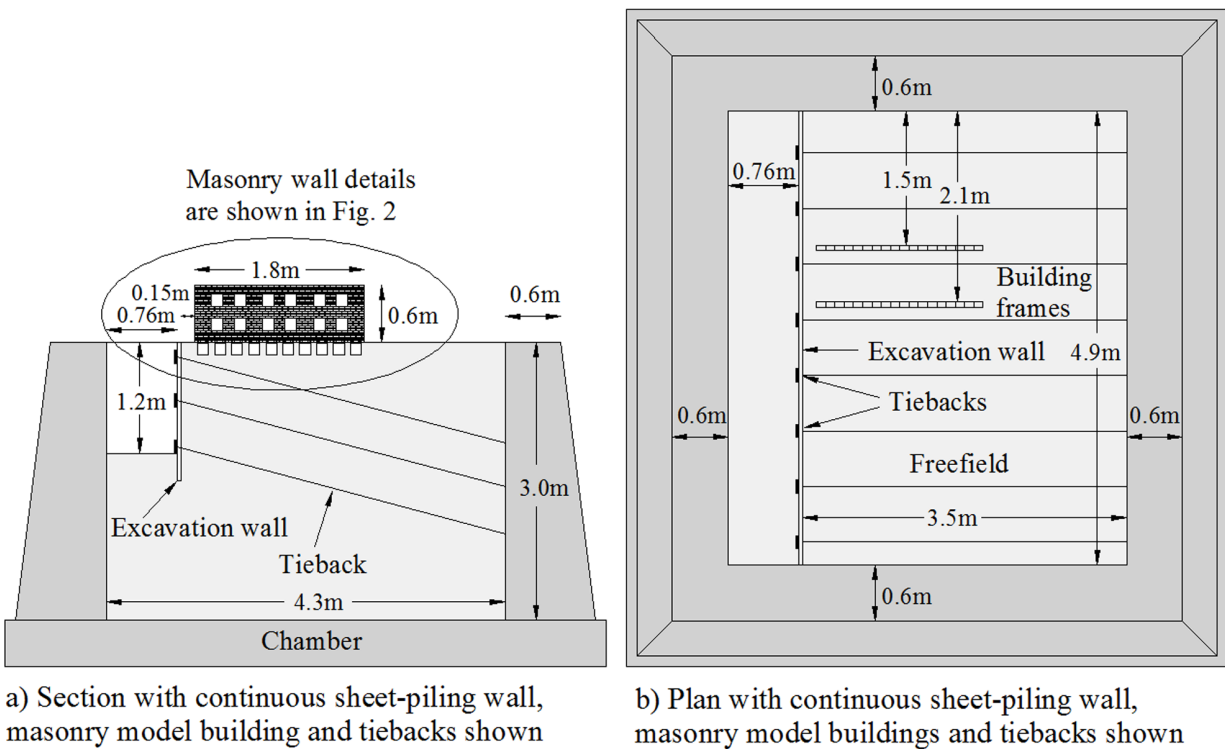


Fig. 1

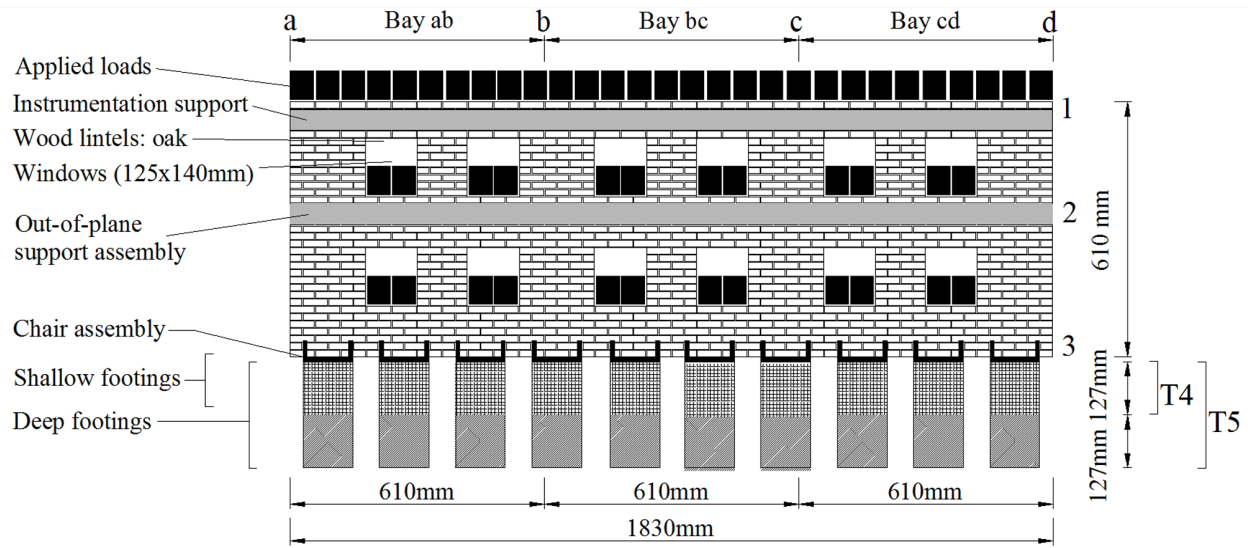


Fig. 2

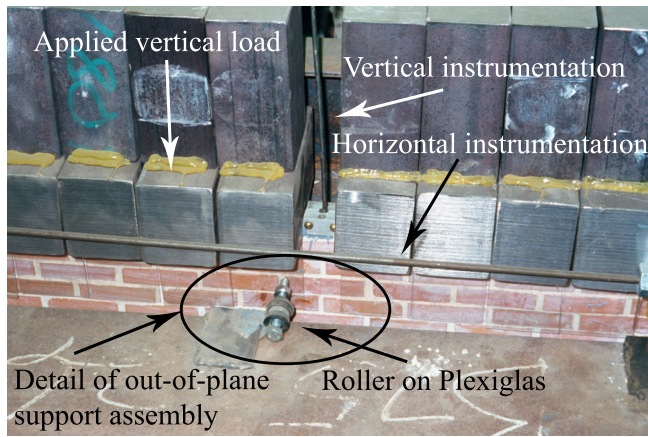


Fig. 3

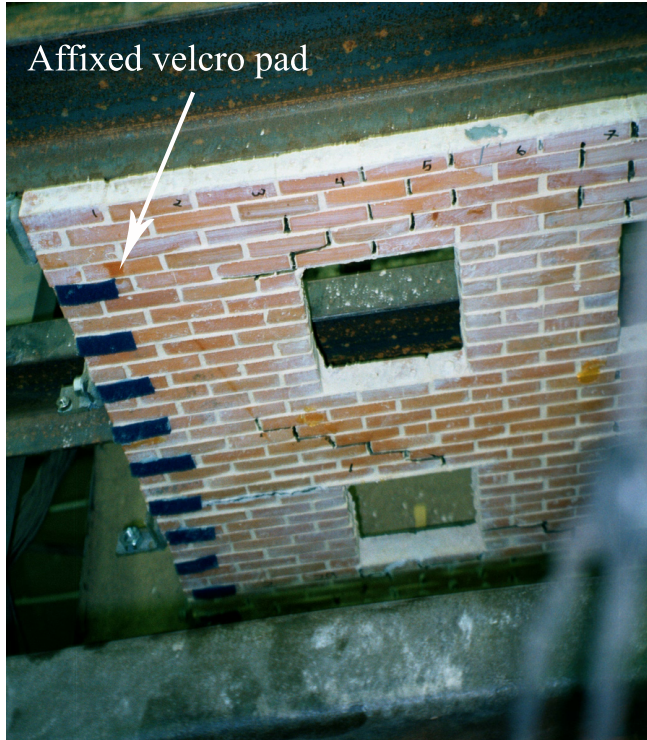


Fig. 4

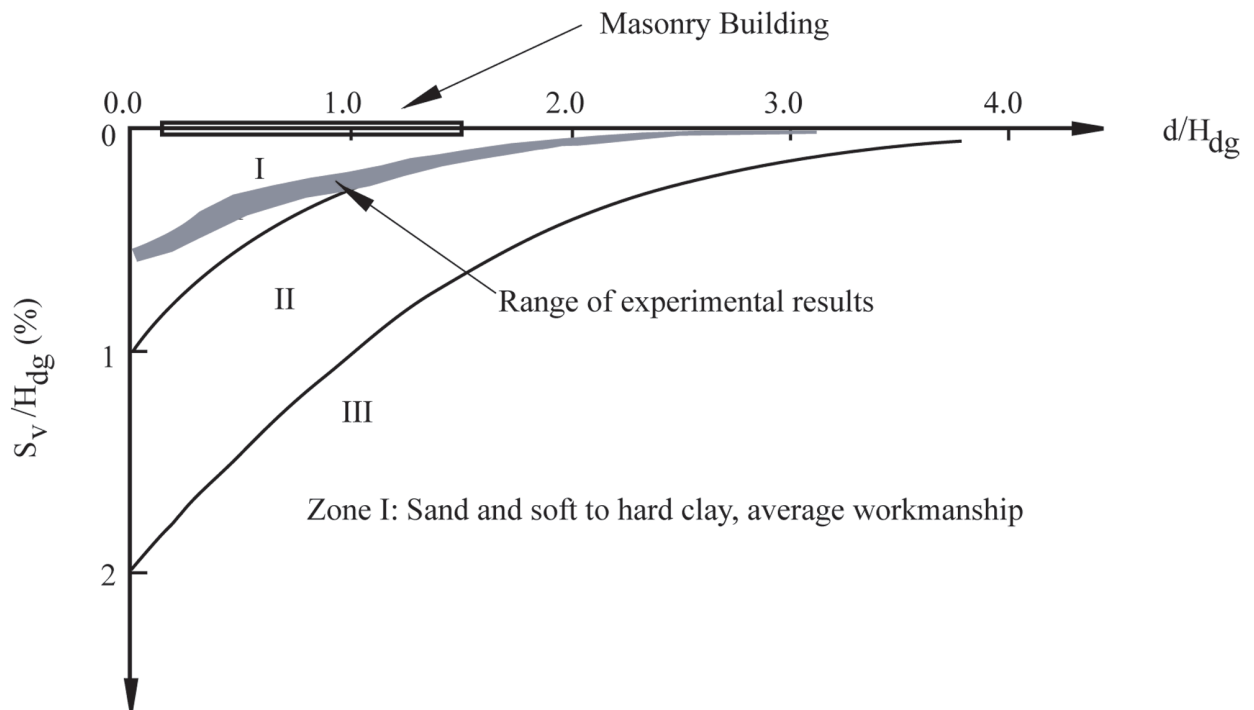


Fig. 5

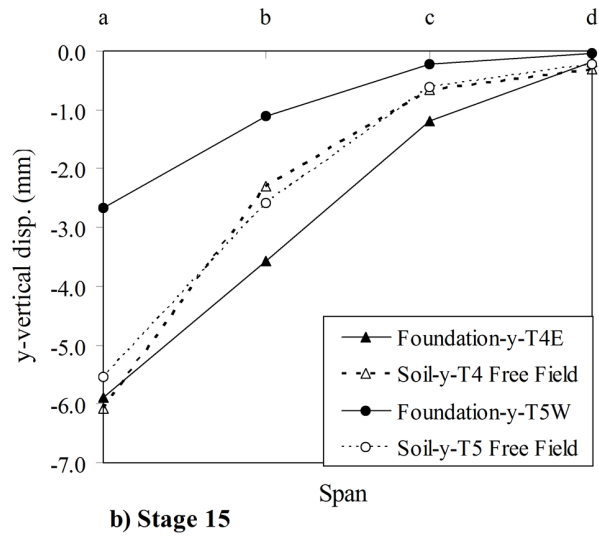
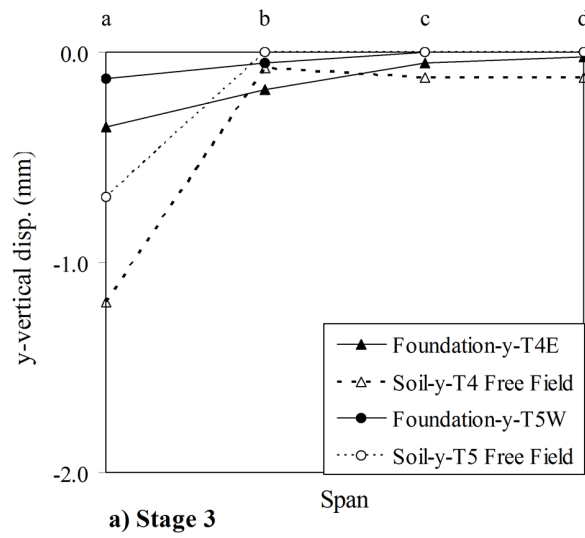


Fig. 6

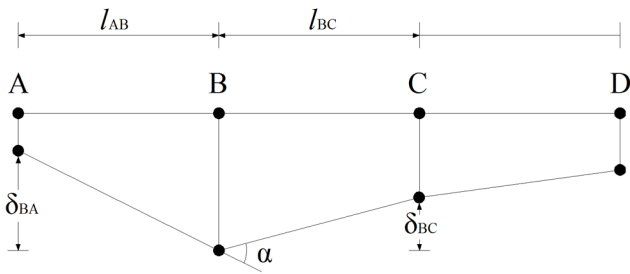


Fig. 7

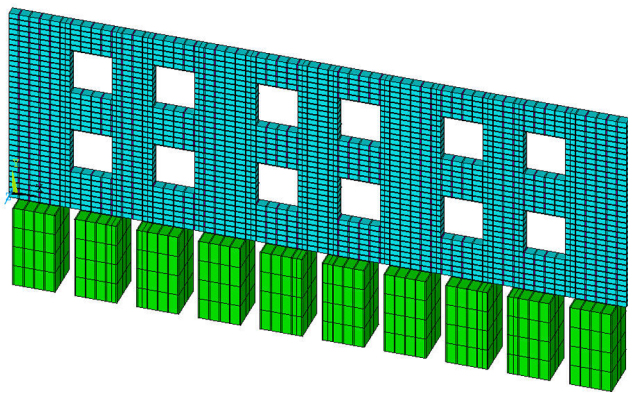


Fig. 8

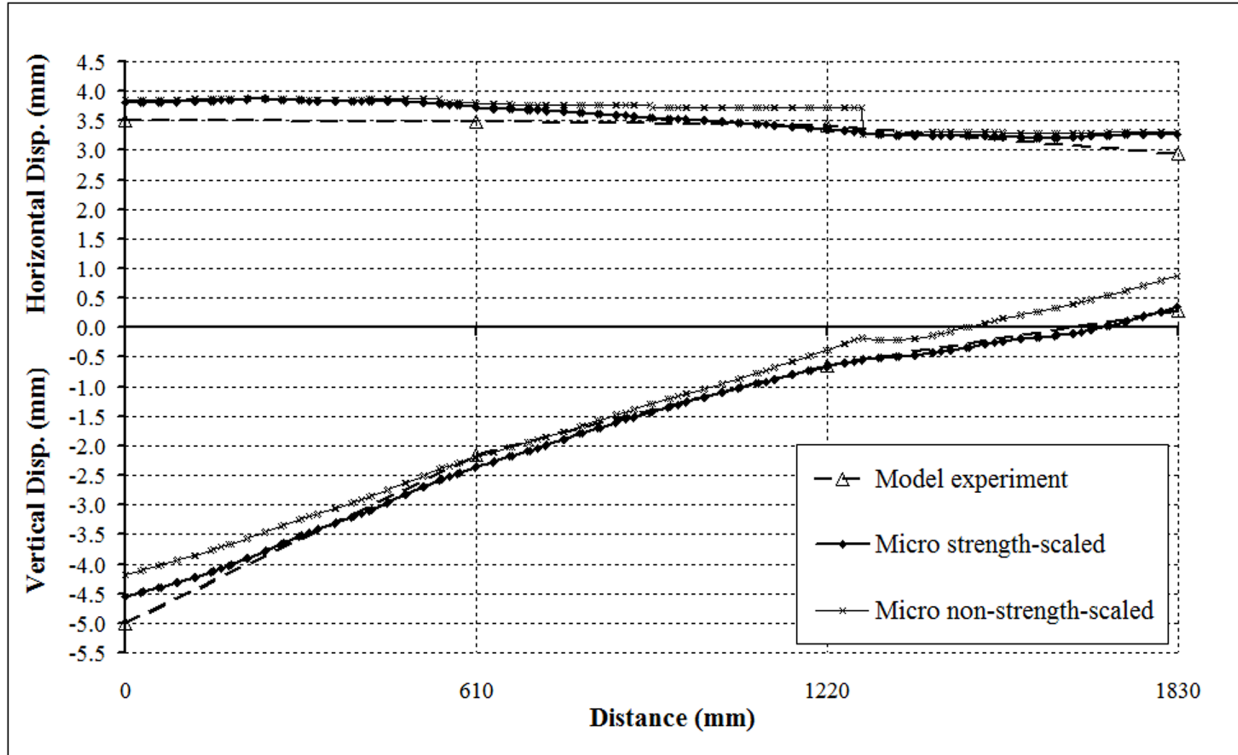


Fig. 9

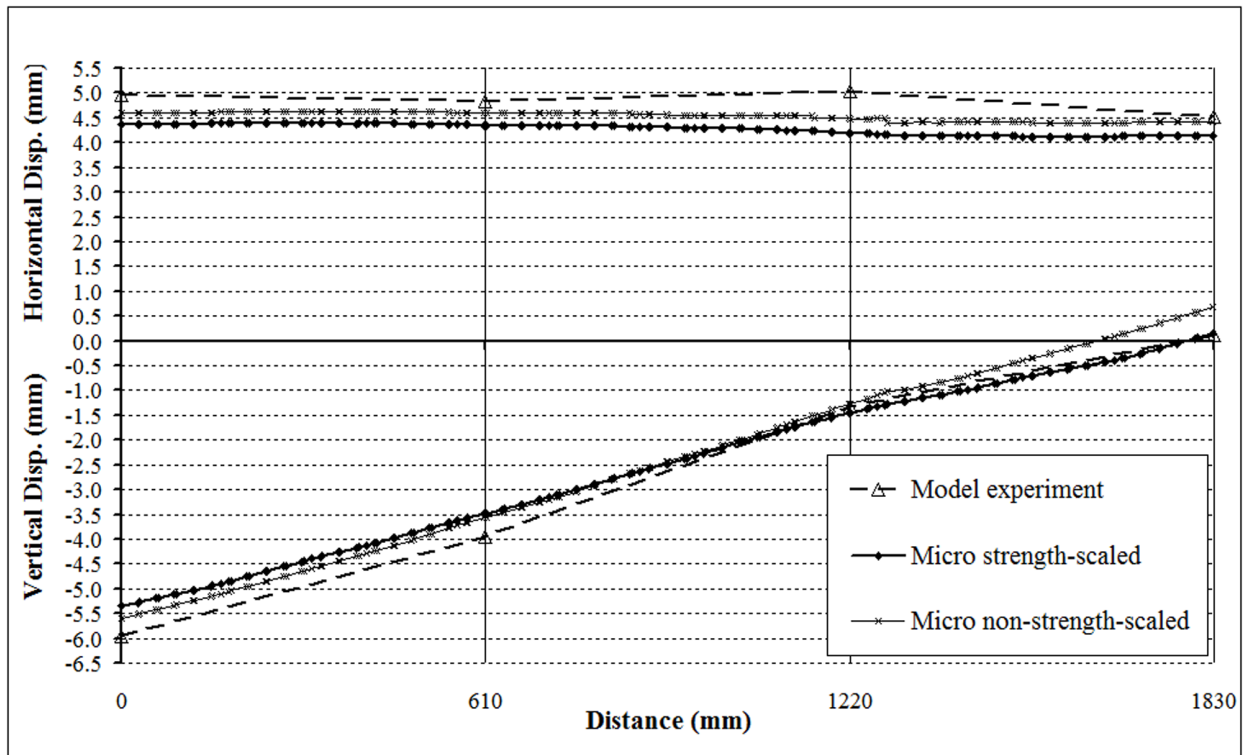


Fig. 10